Enzymology:

Crystal Structure of 3-Hydroxybenzoate 6-Hydroxylase Uncovers Lipid-assisted Flavoprotein Strategy for Regioselective Aromatic Hydroxylation

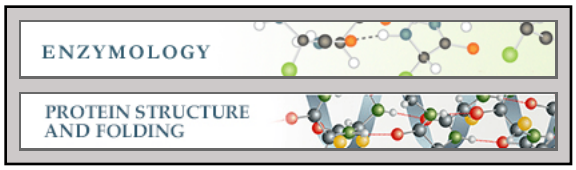

Stefania Montersino, Roberto Orru, Arjan Barendregt, Adrie H. Westphal, Esther van Duijn, Andrea Mattevi and Willem J. H. van Berkel

J. Biol. Chem. 2013, 288:26235-26245.
doi: 10.1074/jbc.M113.479303 originally published online July 17, 2013

THE JOURNAL OF BIOLOGICAL CHEMISTRY VOL. 288, NO. 36, pp. 26235–26245, September 6, 2013

Crystal Structure of 3-Hydroxybenzoate 6-Hydroxylase Uncovers Lipid-assisted Flavoprotein Strategy for Regioselective Aromatic Hydroxylation*

Received for publication, April 25, 2013, and in revised form, July 13, 2013 Published, JBC Papers in Press, July 17, 2013, DOI 10.1074/jbc.M113.479303

Stefania Montersino[‡1], Roberto Orru[§1,2], Arjan Barendregt[¶], Adrie H. Westphal[‡], Esther van Duijn[¶], Andrea Mattevi[§3], and Willem J. H. van Berkel[‡4]

From the [‡]Laboratory of Biochemistry, Wageningen University, 6703 HA Wageningen, The Netherlands, [§]Department of Biology and Biotechnology, University of Pavia, Via Ferrata 9, 27100 Pavia, Italy, and [¶]Biomolecular Mass Spectrometry and Proteomics, Bijvoet Center for Biomolecular Research, and Utrecht Institute for Pharmaceutical Sciences, Utrecht University, Padualaan 8, 3584 CH Utrecht, The Netherlands

Background: 3-Hydroxybenzoate 6-hydroxylase (3HB6H) is a flavoprotein monooxygenase involved in the catabolism of aromatic compounds in soil microorganisms.
Results: The enzyme crystal structure features natively bound phospholipids and a Tyr-His pair for substrate binding and catalysis.
Conclusion: 3HB6H has a peculiar substrate-binding site that uses a bound lipid to help to discriminate between *ortho*- and *para*-hydroxylation.
Significance: 3HB6H structure uncovers new flavoprotein strategy for regioselective aromatic hydroxylation.

3-Hydroxybenzoate 6-hydroxylase (3HB6H) from *Rhodococcus jostii* RHA1 is a dimeric flavoprotein that catalyzes the NADH- and oxygen-dependent *para*-hydroxylation of 3-hydroxybenzoate to 2,5-dihydroxybenzoate. In this study, we report the crystal structure of 3HB6H as expressed in *Escherichia coli*. The overall fold of 3HB6H is similar to that of *p*-hydroxybenzoate hydroxylase and other flavoprotein aromatic hydroxylases. Unexpectedly, a lipid ligand is bound to each 3HB6H monomer. Mass spectral analysis identified the ligand as a mixture of phosphatidylglycerol and phosphatidylethanolamine. The fatty acid chains occupy hydrophobic channels that deeply penetrate into the interior of the substrate-binding domain of each subunit, whereas the hydrophilic part is exposed on the protein surface, connecting the dimerization domains via a few interactions. Most remarkably, the terminal part of a phospholipid acyl chain is directly involved in the substrate-binding site. Co-crystallized chloride ion and the crystal structure of the H213S variant with bound 3-hydroxybenzoate provide hints about oxygen activation and substrate hydroxylation. Essential roles are played by His-213 in catalysis and Tyr-105 in substrate binding. This phospholipid-assisted strategy to control regioselective aromatic hydroxylation is of relevance for optimization of flavin-dependent biocatalysts.

Flavoprotein hydroxylases are involved in diverse biological processes ranging from lignin degradation to the synthesis of polyketide antibiotics (1, 2). They perform regioselective *ortho*- or *para*-hydroxylation reactions on a narrow subset of substrates with tightly regulated oxygen and coenzyme consumption. The reaction cycle of flavoprotein hydroxylases consists of two half-reactions (3). In the reductive half-reaction, the oxidized flavin of the enzyme-substrate complex gets reduced by NAD(P)H. The oxidative half-reaction involves the reaction of reduced FAD with oxygen, the hydroxylation of the substrate, and the regeneration of oxidized flavin. Most biochemically characterized flavoprotein hydroxylases act on monophenols, but the structural basis of this selectivity is unclear (1). Members with known three-dimensional structure include *p*-hydroxybenzoate hydroxylase (PHBH)[5] (4), phenol hydroxylase (5), and 3-hydroxybenzoate 4-hydroxylase (3HB4H) (6). More recently, structural data have become available on flavoprotein hydroxylases that are active with pyridines (7, 8), phenazines (9), and polyketides (10–13).

The Gram-positive actinomycete *Rhodococcus jostii* RHA1 is a rich source of flavoprotein hydroxylases (14). Together with the genera *Nocardia*, *Corynebacterium*, and *Mycobacterium*, *Rhodococcus* forms a distinct group of bacteria called mycolata (15–17). These species are characterized by a complex cell envelope and an impressive catabolic diversity, permitting them to adapt to different carbon sources (18). In comparison with other mycolata, *R. jostii* RHA1 is particularly rich in oxygenases (203 putative genes), gained primarily through ancient gene duplications or acquisitions (19).

* This work was supported by the Integrated Biosynthesis Organic Synthesis program of the Netherlands Organization for Scientific Research (NWO).
The atomic coordinates and structure factors (codes 4BJY, 4BJZ, 4BK1, 4BK2, and 4BK3) have been deposited in the Protein Data Bank (http://wwpdb.org/).
[1] Both authors contributed equally to this work.
[2] Present address: Dept. of Biochemistry, Emory University, Atlanta, GA 30322.
[3] To whom correspondence may be addressed. Tel.: 39-0382-985525; Fax: 39-0382-528496; E-mail: andrea.mattevi@unipv.it.
[4] To whom correspondence may be addressed: Laboratory of Biochemistry, Wageningen University, Dreijenlaan 3, 6703 HA Wageningen, The Netherlands. Tel.: 31-317-482861; Fax: 31-317-484801; E-mail: willem.vanberkel@wur.nl.

[5] The abbreviations used are: PHBH, *p*-hydroxybenzoate hydroxylase; 3HB6H, 3-hydroxybenzoate 6-hydroxylase; 3HB4H, 3-hydroxybenzoate 4-hydroxylase; Bis-Tris, 2-[bis(2-hydroxyethyl)amino]-2-(hydroxymethyl)propane-1,3-diol.

3-Hydroxybenzoate 6-hydroxylase (3HB6H) from *R. jostii* RHA1 participates in the gentisate pathway where it catalyzes the *para*-hydroxylation of 3-hydroxybenzoate to gentisate (Fig. 1). We recently established that 3HB6H is a dimeric flavoprotein with each subunit containing a tightly but non-covalently bound FAD.

3HB6H uses NADH as an electron donor and features narrow substrate specificity. Besides 3-hydroxybenzoate, the enzyme converts a limited number of 3-hydroxybenzoate analogs to the corresponding gentisates (14).

Here we present the crystal structure of 3HB6H refined at 1.51-Å resolution, which reveals that the protein harbors natively bound phospholipids. We found that 3HB6H shares a common fold with other flavoprotein hydroxylases and that the domain architecture and topology is closest to family members that catalyze *para*-hydroxylation reactions. To gain insight into the structural determinants of the regioselectivity of flavoprotein-dependent 3-hydroxybenzoate hydroxylation, we addressed the mode of substrate binding in 3HB6H and the role of putative active site residues in catalysis. The results uncover a strategy in which a flavoprotein monooxygenase uses a phospholipid chain and properly positioned residues to achieve regioselective *para*-hydroxylation.

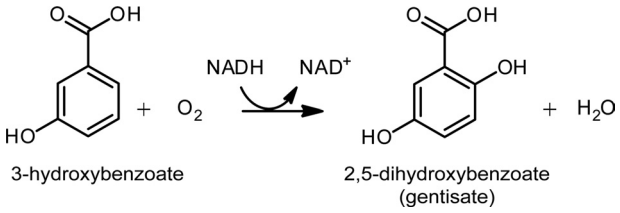

FIGURE 1. **Reaction catalyzed by 3HB6H.**

EXPERIMENTAL PROCEDURES

Chemicals—*Pfu* DNA polymerase, DpnI, and dNTPs were purchased from Invitrogen. Oligonucleotides were synthesized by Eurogentec (Liege, Belgium). *Escherichia coli* TOP10 was from Invitrogen. Aromatic compounds were purchased from Sigma-Aldrich and Acros Organics (Fair Lawn, NJ). Crystallization kits were purchased from New Hampton (Aliso Viejo, CA). All other chemicals were from commercial sources and of the purest grade available.

Cloning and Site-directed Mutagenesis—3HB6H variants were constructed using pBAD-3HB6H-His$_6$ as template using the QuikChange I protocol (Stratagene, La Jolla, CA). Oligonucleotides used were Y105F_fw (5′-GCTACGGCGGACCGTTTTTCGTGACCCATCG-3′), H213A_fw (5′CGGACCGCGGTGCGCATTCATCCAGTACCC-3′), H213S_fw (5′CGGACCGCGGTGCTCATTCATCCAGTACCC-3′), and Q301E_fw (5′-GCACCCGCCACTGGAATACCTGGCCTCG-3′) with the codon exchanged underlined. Successful mutagenesis was confirmed by automated sequencing. Resulting constructs were electroporated to *E. coli* TOP10 (Invitrogen) for recombinant expression.

Protein Production—3HB6H from *R. jostii* RHA1 and 3HB6H variants were expressed in *E. coli* and purified as C-terminal His$_6$-tagged protein as described previously (14).

Crystallization and Structure Determination—Crystals for structure determination were obtained by the sitting drop vapor diffusion method at 20 °C by mixing equal volumes (2 μl) of protein and reservoir solutions. Protein solutions consisted of 30 mg of enzyme/ml (0.625 mM) in 1 mM FAD, 2 mM 3-hydroxybenzoate, and 50 mM Bis-Tris (pH 7.2), whereas precipitant solutions consisted of 28% PEG 4000, 0.2 M sodium acetate, and 0.1 M Tris-HCl (pH 8.5). Yellow crystals grew in 1 day. A platinum derivative was obtained by soaking the 3HB6H crystals for 16 h in 20 μl of reservoir solution containing 0.5 mM

TABLE 1
Crystallographic data collection and refinement statistics
r.m.s., root mean square; r.m.s.d., root mean square deviation.

	Platinum derivative	Wild type	H213S	Q301E	Y105F
Protein Data Bank code	4BJY	4BJZ	4BK1	4BK2	4BK3
Beamline	PX1-X06SA	Proxima1	ID14eh4	ID14eh4	ID14eh4
Unit cell (Å)	$a = b = 106.6$, $c = 142.3$	$a = b = 106.8$, $c = 142.7$	$a = b = 105.8$, $c = 142.3$	$a = b = 106.8$, $c = 142.7$	$a = b = 106.4$, $c = 142.6$
Space group	$I4_122$	$I4_122$	$I4_122$	$I4_122$	$I4_122$
Resolution (Å)	1.52	1.51	1.73	2.47	1.78
Wavelength (Å)	0.934	0.980	0.976	0.976	0.976
f′	11.68				
f″	16.72				
R_{sym}[a,b] (%)	5.9 (57.6)	8.2 (68.5)	6.1 (20.2)	1.1 (2.4)	13.8 (54.3)
CC½[b,c]	1.00 (0.96)	1.00 (0.55)	0.99 (0.97)	1.00 (0.98)	0.99 (0.83)
CC*[b,c]	1.00 (0.99)	1.00 (0.84)	1.00 (0.99)	1.00 (0.99)	1.00 (0.95)
Completeness[b] (%)	100 (100)	99.2 (99.4)	97.6 (99.3)	99.9 (100)	99.5 (100)
Unique reflections	62,993	63,875	40,940	15,081	39,090
Redundancy[b]	23.7 (24.3)	3.5 (3.6)	3.4 (3.2)	9.4 (9.4)	6.8 (6.4)
I/σ[b]	33.5 (6.6)	7.6 (1.5)	12.3 (4.6)	14.3 (8.4)	7.5 (2.3)
No. of atoms	3,448	3,636	3,527	3,242	3,484
R_{cryst}[d] (%)	17.4	16.8	15.8	17.3	15.9
R_{free}[d] (%)	20.5	20.1	20.1	24.1	20.6
r.m.s. bond length (Å)	0.021	0.019	0.021	0.015	0.020
r.m.s. bond angles (°)	2.10	1.93	2.04	1.65	1.98
r.m.s.d. (Å)			0.1790	0.1829	0.1132
Residues			389	393	395

[a] $R_{sym} = \sum|I_i - I|/\sum I_i$ where I_i is the intensity of ith observation and I is the mean intensity of the reflection.
[b] Values in parentheses are for reflections in the highest resolution shell. CC1/2: Pearson correlation coefficient between the average intensities of each subset. CC*: correlation of observed data set with underlying true signal.
[c] Ref. 28.
[d] $R_{cryst} = \sum|F_{obs} - F_{calc}|/\sum F_{obs}$ where F_{obs} and F_{calc} are the observed and calculated structure factor amplitudes, respectively. R_{cryst} and R_{free} were calculated using the working and test set, respectively.

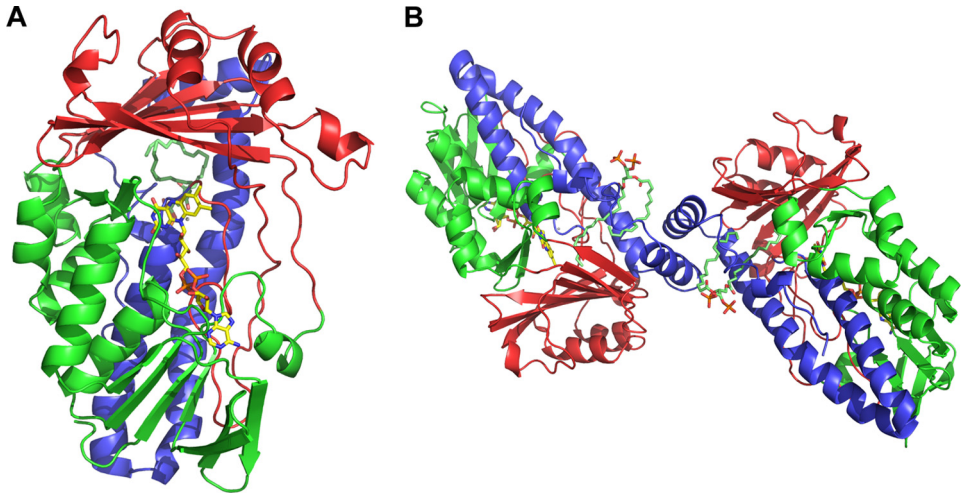

FIGURE 2. **Overall structure of 3HB6H and domains organization.** *A*, schematic view of 3HB6H monomer. *B*, schematic view of 3HB6H dimer. The FAD-binding domain (residues 1–73 and 94–175) is depicted in *green*, substrate-binding domain (residues 74–93 and 176–302) is in *red*, and dimerization domain (residues 303–398) is in *blue*. FAD is shown as a *stick* model with flavin carbon in *yellow*, nitrogens in *blue*, oxygens in *red*, and phosphorous atoms in *brown*. Phosphatidylglycerol is shown as a *stick* model with lipid carbon in *light green*. The solvent-accessible surface area of each monomer buried upon dimer formation is 7200 Å^2.

$K_2Pt(NO_2)_4$ dissolved in DMSO. Crystals of 3HB6H variants were obtained with the same method, temperature, and volumes in a reservoir solution consisting of 30% PEG 4000, 0.2 M $LiSO_4$, and 0.1 M Tris-HCl (pH 8.5). The H213A mutant did not produce good crystals. X-ray diffraction data were collected at the European Synchrotron Radiation Facility synchrotron source (Grenoble, France) and Swiss Light Source (Villigen, Switzerland) and processed with the CCP4 package (20, 21). The structure was solved by the single wavelength anomalous dispersion method by using the pipeline SHELXC/D/E (22) and ARP/wARP for the model building (23) and refined with REFMAC5 (24) and Coot (25). Pictures were generated with the programs PyMOL (26) and CCP4mg (27). Data collection parameters and final refinement statistics are listed in Table 1 (28).

Analytical Methods—Enzyme concentrations were determined by measuring the absorbance of protein-bound FAD (14) using the following molar absorption coefficients: 3HB6H, ϵ_{453} = 10.3 mM^{-1} cm^{-1}; Y105F, ϵ_{450} = 10.4 mM^{-1} cm^{-1}; H213A, ϵ_{457} = 9.8 mM^{-1} cm^{-1}; H213S, ϵ_{451} = 9.9 mM^{-1} cm^{-1}; Q301E, ϵ_{446} = 10.8 mM^{-1} cm^{-1}.

Activity Measurements—3HB6H activity was routinely assayed by following the decrease in absorbance of NADH at 360 nm at 25 °C on a Hewlett-Packard 8453 diode array spectrophotometer. Reactions were performed in 50 mM Tris-SO_4 (pH 8.0) and 10 μM FAD and started by addition of 46 nM enzyme. Initial rates were calculated using a molar absorption coefficient (ϵ_{360}) of 4.31 mM^{-1} cm^{-1} (14). One unit of enzyme activity is defined as the amount of enzyme that consumes 1 μmol of NADH/min.

Oxygen Consumption—An OxyTherm Clark-type oxygen electrode system (Hansatech, Norfolk, UK) was used to determine the hydroxylation efficiency of 3HB6H variants toward different aromatic substrates. The assay solution (final volume, 1.0 ml) contained 350 μM aromatic substrate, 250 μM NADH, and 1–10 μM enzyme in 50 mM air-saturated Tris-SO_4 (pH 8.0) at 25 °C. At the end of the reaction, the amount of hydrogen peroxide produced was determined by adding 20 μg of catalase ($2\ H_2O_2 \rightarrow O_2 + 2\ H_2O$).

TABLE 2
DALI alignment

Protein Data Bank code	Z-score[a]	r.m.s.d.[b]	lali[c]	nres[d]	id[e]	Name[f]
					%	
3RP6	44.5	2.4	371	392	22	HpXO
3ALL	39.8	2.6	346	371	23	MHPCO
3C96	38.9	2.3	341	381	26	PhzS
2VOU	37.1	2.6	349	393	22	DHPH
1D7L	34.6	3.0	352	394	14	PHBH
2Y6Q	34.3	3.2	345	368	15	TetX2
2X3N	33.5	3.1	342	364	20	FAD-dependent monooxygenase
3IHG	32.1	3.1	352	535	15	Aklavinone 11-hydroxylase
3EIT	31.7	3.1	338	437	17	CndH halogenase
3FMW	31.6	3.3	347	489	19	MtmOIV
2DKI	31.5	3.3	341	615	17	3HB4H
3NIX	31.5	3.2	353	407	15	Flavoprotein dehydrogenase
1FOH	30.6	3.1	357	656	14	PHHY

[a] Calculated on DALI server on February 15, 2013 (51).
[b] Root mean square deviation.
[c] Number of aligned positions.
[d] Number of residues in matched structure.
[e] Sequence identify of aligned positions.
[f] HpXO, Urate oxidase; MHPCO, 2-methyl-3-hydroxypyridine-5-carboxylic acid oxygenase; PhzS, phenazine hydroxylase; DHPH, 2,6-dihydroxypyridine 3-hydroxylase; TetX2, tetracycline 11-hydroxylase; CndH halogenase, chondrochloren halogenase; MtmOIV, mithramycin monooxygenase; PHHY, phenol hydroxylase.

Substrate Binding—The interaction of 3HB6H (25 μM) with substrate analogs was studied in 50 mM Tris-SO_4 (pH 8.0). Dissociation constants (K_d) of enzyme-substrate complexes were determined from flavin absorption difference spectra essentially as described elsewhere (14).

Lipid Identification—Identification of protein-bound lipids was performed as follows. Extraction of lipids was achieved by mixing 100 μl of buffer-exchanged protein solution (50 mM ammonium acetate (pH 6.8)) with 267 μl of chloroform and 133 μl of methanol in a glass reaction tube. Once phase separation

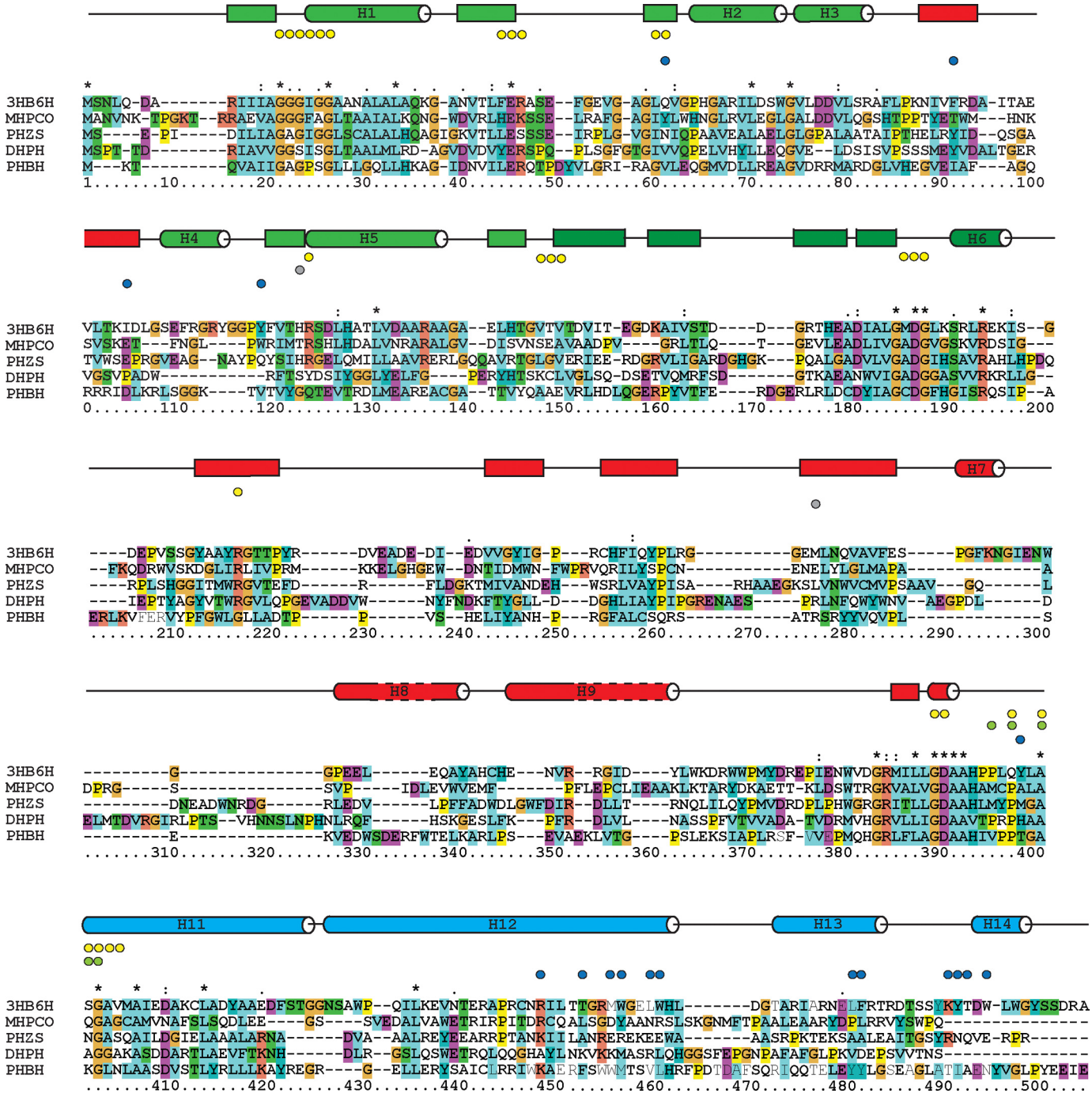

FIGURE 3. **Structure-based sequence alignment of flavoprotein aromatic hydroxylases.** From *top*, 3HB6H, 2-methyl-3-hydroxypyridine-5-carboxylic acid oxygenase (*MHPCO*; Protein Data Bank code 3ALL), flavin-containing monooxygenase PhzS (Protein Data Bank code 3C96), 2,6-dihydroxypyridine-3-hydroxylase (*DHPH*; Protein Data Bank code 2VOU), and PHBH (Protein Data Bank code 1D7L) are shown. Secondary structure elements of 3HB6H are indicated above the alignment and are colored according to the respective domain (see Fig. 2). Residues involved in direct FAD contact (*yellow circles*), chloride contact (*green circles*), and lipid contact (*blue circles*) are indicated. Conservation of amino acid residues in fingerprint sequences: identical residues (*), conserved substitutions (:), semi-conserved substitutions (.). 3HB6H and PHBH residues involved in dimerization are in *regular font*. Shading of amino acid residues depends on their chemical characteristics. Structural alignment was done by STRAP (52) and edited in ClustalW (53).

was reached, the chloroform phase was extracted using a Pasteur pipette and collected in a new reaction tube. Evaporation of the organic phase was done by flushing with nitrogen gas, and the dry sample was dissolved in 15 μl of isopropanol and analyzed.

Electrospray ionization-MS or -MS/MS analysis of lipid identification was performed on a Quattro Ultima nanoflow triple quadrupole mass spectrometer (Micromass, Manchester, UK) equipped with a Z-spray nanoelectrospray ionization source. All measurements were performed by operating in the positive and negative ion modes using gold-coated needles made with borosilicate glass capillaries (Kwik-Fill, World Precision Instruments, Sarasota, FL) on a P-97 puller (from Sutter Instruments, Novato, CA). The needles were coated with a gold

layer, which was performed by an Edwards Scancoat Six Pirani 501 sputter coater (Edwards Laboratories, Milpitas, CA). Mass spectra were recorded with a capillary voltage of 1.3 kV and a cone voltage of 150 V. For MS/MS, argon was supplied in the collision cell (2.0×10^{-3} mbar). Collision energy was adjusted to gain optimal fragmentation.

RESULTS

Overall Structure of 3HB6H—The structure of 3HB6H was solved at 1.51-Å resolution using the single wavelength anomalous dispersion method (Table 1). The final model of 3HB6H monomer (Fig. 2) contains one molecule of FAD, one chloride ion, and a phospholipid ligand. All protein residues (except the N-terminal 1–2 residues and C-terminal 25 residues containing a spacer and the His_6 tag) have well defined ordered conformations. The three-dimensional structure of 3HB6H is similar to that of PHBH and other flavoprotein hydroxylases (1, 2). A DALI structural homolog search (Table 2) revealed that despite a relatively low sequence identity (14–26%) most parts of the protein could be structurally aligned with related flavoprotein hydroxylases (Fig. 3).

FAD-binding Domain—The FAD-binding domain contains a Rossmann fold for binding the ADP moiety of the cofactor. The isoalloxazine ring of FAD is located in the interior of the protein at the interface between the FAD- and substrate-binding domains. FAD contacts around 30 residues along the polypeptide chain (Figs. 3 and 4*A*), resulting in a tight protein-cofactor interaction. One-third of the protein-FAD contacts are strictly conserved among flavoprotein hydroxylases and cluster around the three fingerprint sequences (29).

For PHBH, it was observed that the isoalloxazine ring of FAD occupies different conformations: *in*, *out*, and *open* (30, 31). The *out* conformation enables flavin reduction, the *in* conformation ensures substrate hydroxylation during the oxidative half-reaction, and the *open* conformation allows substrate/product binding and release. In 3HB6H, the flavin ring has a well defined electron density and was refined with full occupancy in the *in* conformation (Fig. 4*A*), similarly to the FAD conformation of the substrate-free forms of 2-methyl-3-hydroxypyridine-5-carboxylic acid oxygenase and 2,6-dihydroxypyridine 3-hydroxylase. Earlier studies with PHBH have indicated that the FAD domain plays a crucial role in NADPH binding (32, 33) and that a small helix near the protein surface is the key determinant for the coenzyme specificity (34). The absence of this surface helix in 3HB6H does not explain the NADH preference of the enzyme.

Substrate-binding Domain—The active site of 3HB6H is formed by residues of the FAD- and substrate-binding domains. Although wild-type 3HB6H crystals were prepared with excess 3-hydroxybenzoate in the crystallization drop, no electron density for the aromatic substrate was found in the active site (Fig. 4*A*). Crystals contain a chloride ion interacting with Gln-301, Ala-304, and Gly-306 at 4-Å distance from flavin C4a.

Dimerization Domain—3HB6H is a dimer both in solution (14) and in the crystal form (Fig. 2*B*). Among structurally related proteins, PHBH shows similar dimer association. PHBH uses three helices to form a hydrophobic dimerization interface

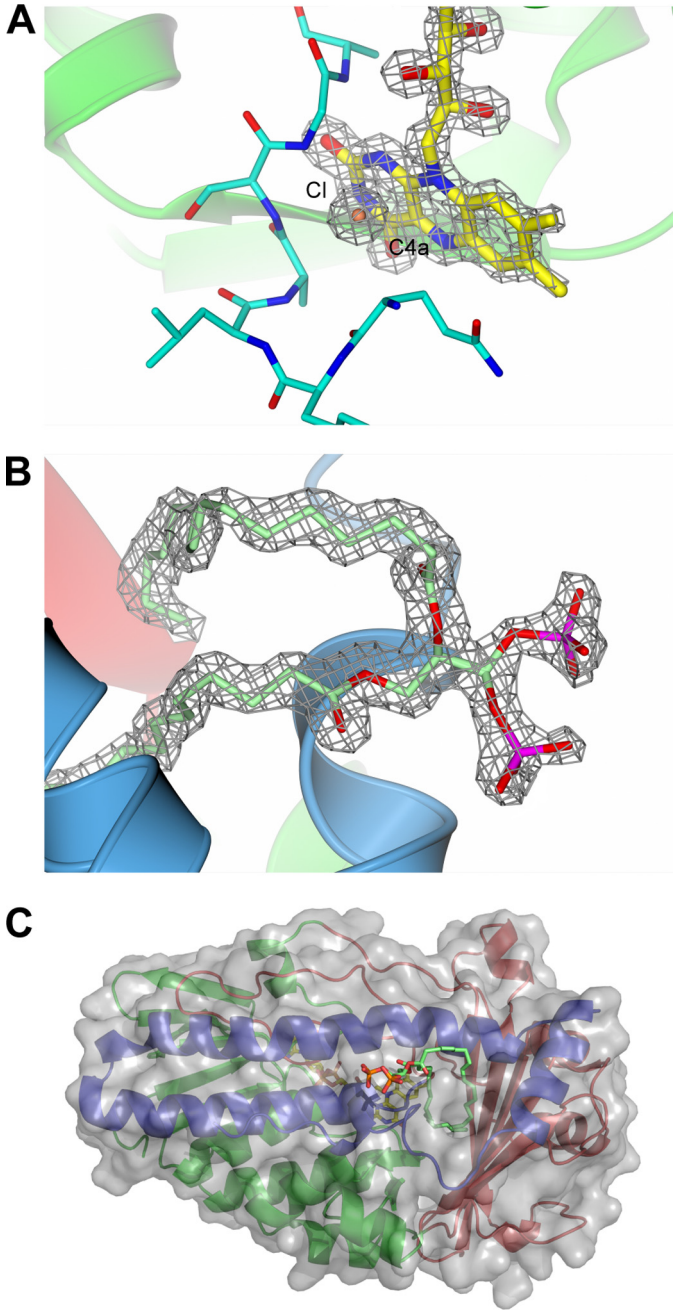

FIGURE 4. **Detailed view of cofactor binding, active site, and lipid-binding site of 3HB6H.** *A*, weighted $2F_o - F_c$ electron density of FAD contoured at 1.5σ. The bound chloride is represented as an *orange sphere*. Residues involved in chloride binding are depicted as *sticks*. The C4a atom of the flavin is labeled. FAD is shown as a *stick* model with flavin carbons in *yellow*, nitrogens in *blue*, oxygens in *red*, and phosphorous atoms in *brown*. *B*, stick representation of natively bound lipids in the weighted $2F_o - F_c$ electron density map contoured at 1.5σ. Phosphatidylglycerol is shown as a *stick* model with carbons in *light green*, nitrogens in *blue*, oxygens in *red*, and phosphorous atoms in *purple*. *C*, 3HB6H surface representation (transparency, 0.2) with lipid represented as *sticks*.

with a few salt bridges (35, 36). Compared with PHBH, in 3HB6H, there are fewer intermonomer contacts, and dimer interactions occur mainly via one helix (H12H13* and H13H13*) (Figs. 2*B* and 3).

Lipid Binding and Identification—Electron density of a lipid-like ligand was observed in all 3HB6H structures (Fig. 4, *B* and *C*). Tentatively, a phospholipid with two chains of 16 carbons

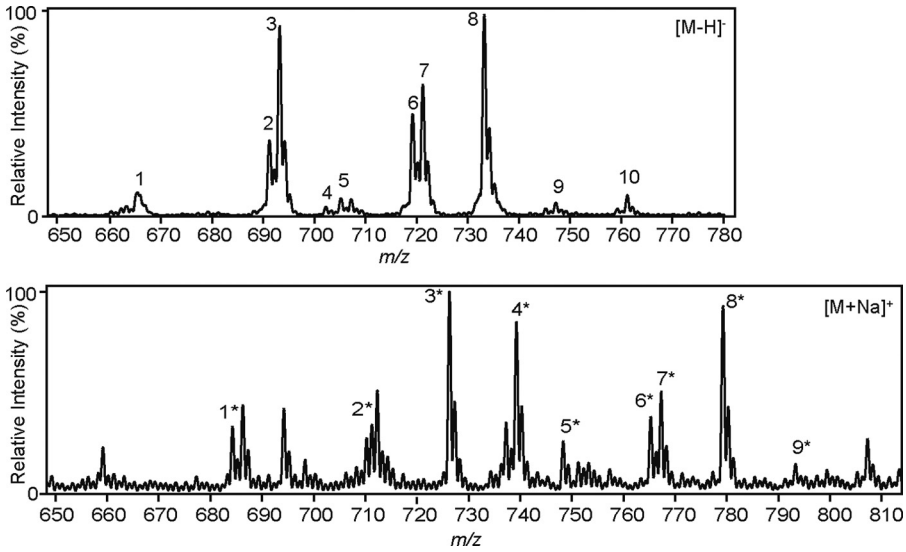

FIGURE 5. **Lipid identification by mass spectrometry.** Electrospray ionization-MS spectrum of extracted lipids in negative mode (*top panel*) and positive mode (*bottom panel*). Natively bound lipids of 3HB6H are shown in the mass range 650–810 *m/z*. Identification of the *numbered peaks* is listed in Table 4.

was modeled on the basis of the electron density in the difference Fourier map (Fig. 4*B*). The lipid is inserted in a tunnel, which runs from the protein surface to the active site (Fig. 4*C*). In the tunnel, the lipid contacts hydrophobic and aliphatic residues. Some interaction occurs between the phospholipid and the opposite monomer (Fig. 2*B*). From the crystal structure, the exact identity of the phospholipid was difficult to assign as the density of the headgroup is poorly defined. Detailed assignment of the phospholipid was achieved by mass spectral analysis of the low molecular weight components extracted from denatured 3HB6H. The mass spectrum (Fig. 5) showed four main peaks with *m*/*z* values of 693, 719, 721, and 733 (Fig. 5, *peaks 3* and *6–8*) in the negative mode and three main peaks in the positive mode with *m*/*z* values of 726, 739, and 779, respectively (Fig. 5, *peaks 3**, *4**, and *8**). Fragmentation analysis and comparison with *E. coli* lipid MS spectra (37–40) led to the matching of the mass peaks with either phosphatidylglycerol or phosphatidylethanolamine with aliphatic chains ranging from 14 to 19 carbons (Table 3). Phosphatidylglycerols were visible both in negative and positive modes as complexes with two sodium molecules, whereas phosphatidylethanolamines in the positive mode mostly were found in complex with one sodium ion.

TABLE 3
Lipid identification by mass spectrometry
PG, phosphatidylglycerol; PE, phosphatidylethanolamine; ND, not determined; cy, cyclic.

MS mode	*m*/*z*	[M − H]	Abbreviation
[M − H]			
1	665		PG C14:0/C14:0
2	691		PG C14:0/C16:1
3	693		PG C14:0/C14:0
4	702		PE C16:0/cyC17:0
			PG C14:0/cyC17:0
5	705		PG C15:0/C16:1
			PG C14:0/C18:1
6	719		PG C15:0/cyC17:0
			PG C16:0/C16:1
7	721		PG C16:0/C16:0
8	733		PG C16:0/cyC17:0
9	747		PG C16:0/C18:1
10	761		PG C16:0/cyC19:0
[M + H][a]			
1*	684	ND	PE C14:0/C16:1 (661)
2*	711	1	
3*	726	4	
4*	739	3	
5*	748	4	
6*	765	6	
7*	767	7	
8*	779	8	
9*	793	9	

[a] Peaks 1* and 3* contain one sodium ion; the other peaks contain two sodium ions. Parenthetical value represents mass of peak 1* without sodium ion.

Investigation of Substrate Binding and Catalytic Residues—Putative active site residues and orientation of the substrate were initially inferred from comparison of the native 3HB6H structure with those of other flavoprotein hydroxylases (Fig. 6). Based on these structural comparisons, we hypothesized that residues Tyr-105, His-213, and Gln-301 could be predictably involved in binding of the substrate, especially in the interactions with its carboxylate and hydroxyl groups. To probe the role of these catalytic residues, the enzyme variants Y105F, H213A, H213S, and Q301E were expressed and purified. The mutant proteins were analyzed for their catalytic and binding properties with 3-hydroxybenzoate (Table 4 and Fig. 7). Compared with wild-type enzyme, Y105F showed less affinity for the aromatic substrate with a 14-fold increase in K_d (Fig. 7). Weaker substrate binding does not affect the hydroxylation efficiency (>90% coupling) and turnover rate. Due to a 4-fold higher apparent K_m, Y105F has a lower specificity constant (k_{cat}/K_m) than wild-type enzyme. H213A turned out to be inactive. No NADH oxidation was observed under standard assay conditions, although at very high (10 μM) enzyme concentrations, NADH was slowly consumed. Intriguingly, the strength of substrate binding is not affected by the His-213 → Ala replacement (Fig. 7*B* and Table 4). H213S and Q301E were also inactive (Table 4). With these variants, no characteristic perturbations in the absorption spectrum of protein-bound FAD occurred in the presence of 3-hydroxybenzoate (Fig. 7*A*).

Crystal structures were obtained of Y105F, H213S, and Q301E (Table 1). The H213S mutant shows a small modification in the active site structure with the side chain of Gln-301 rotating away from the conformation present in the wild-type

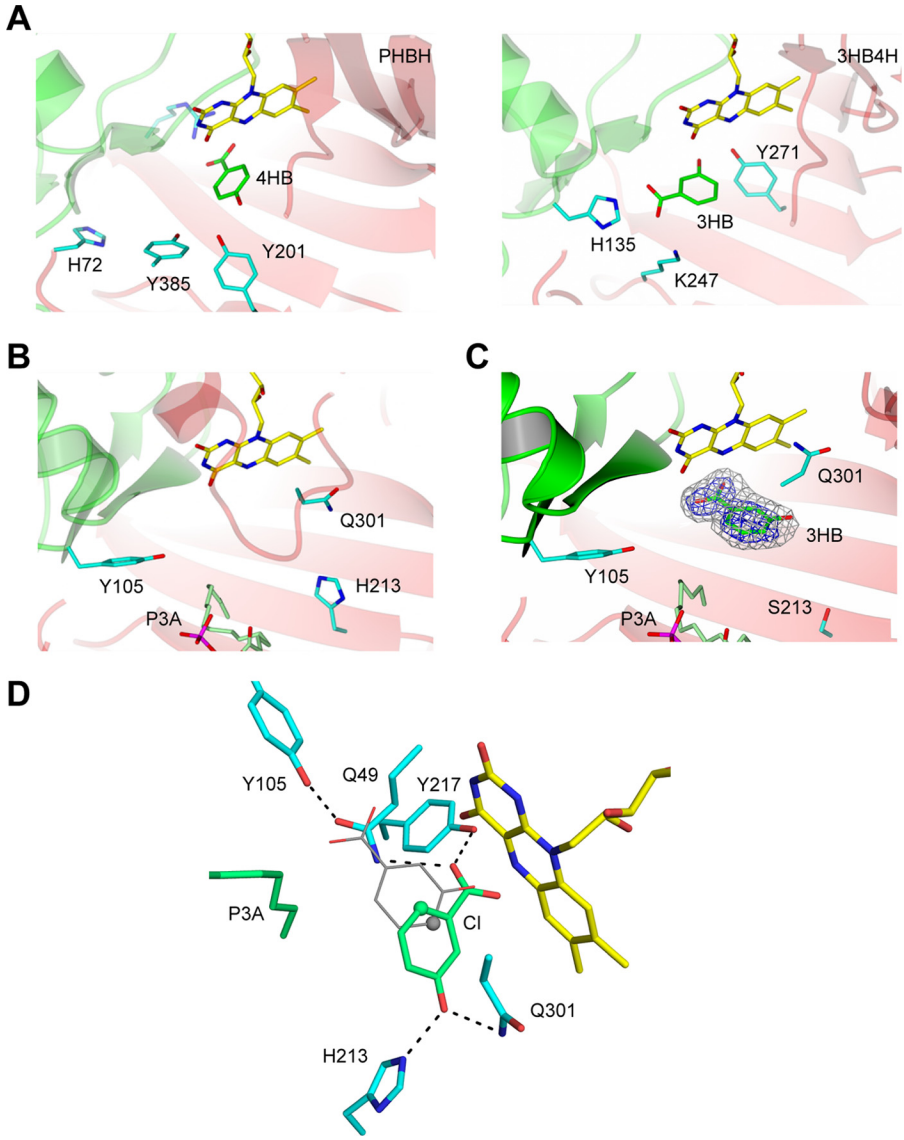

FIGURE 6. **Substrate-binding site in 3HB6H and other FAD-dependent aromatic hydroxylases.** *A*, PHBH (Protein Data Bank code 1PBE) and 3HB4H (Protein Data Bank code 2DHK) active site. FAD is shown as a *stick* model with flavin carbons in *yellow*, nitrogens in *blue*, and oxygens in *red*. The FAD is in the *in* conformation. Aromatic substrate is shown as a *stick* model with carbons in *green* and oxygens in *red*. Residues important for substrate binding are depicted as *stick* models with carbons in *cyan*, nitrogens in *blue*, and oxygens in *red*. *B*, close-up view of the wild-type 3HB6H active site approximately in the same orientation as those of PHBH and 3HB4H shown in *A*. Bound phospholipid (*P3A*) is shown as a *stick* model with carbons in *light green*, oxygens in *red*, and phosphorous atoms in *purple*. *C*, H213S active site with bound 3-hydroxybenzoate in the weighted $2F_o - F_c$ electron density map contoured at 1.4σ (*blue*) and 0.9σ levels. The electron density indicates that the substrate is bound with two conformations (*i.e.* rotation around the C1-C4 axis) that were refined with the atomic occupancies set to a 0.5 value for all substrate atoms. *D*, 3HB6H active site with bound 3-hydroxybenzoate as observed in the structure of the H213S mutant. The figure also shows the position of the substrate as bound in 3HB4H (*gray* carbons; generated by superposing 3HB4H onto 3HB6H Cα atoms). Possible H-bonds are shown as *dashed lines*. The sites of hydroxylation (C4 in 3HB4H and C6 in 3HB6H) are indicated by *spheres*.

TABLE 4

Kinetic parameters and 3-hydroxybenzoate binding of 3HB6H variants

Data are presented as the mean ± S.D. of at least two independent experiments. —, no binding observed.

Enzyme	K_d	K_m	k_{cat}
	μM	μM	s^{-1}
Wild type	48 ± 2	27 ± 3	36 ± 1
Y105F	644 ± 53	186 ± 22	41 ± 2
H213A	61 ± 5	—	Inactive
H213S	—	—	Inactive
Q301E	—	—	Inactive

enzyme (Fig. 6, *B* and *C*). Furthermore, although all variants were crystallized in the presence of 3-hydroxybenzoate, H213S crystals were the only ones to contain a bound substrate (Fig. 6*C*). The ligand carboxylate group is H-bonded to Gln-49 and Tyr-217, whereas the phenyl ring interacts with the C4a-N5 locus of the flavin, the terminal part of a phospholipid aliphatic chain, and Ser-213. As gathered from the electron density, the substrate binds in two conformations flipped by 180° around the C1-C4 axis of the aromatic ring (Fig. 6*C*). The double orientation is likely to be a consequence of the disruption of the anchoring point for the substrate 3-hydroxyl group caused by the H213S mutation and the conformational change of Gln-301 (Fig. 6, *B*–*D*). This feature may also explain why this mutant exhibits no spectroscopic perturbation upon substrate binding, although, at least in the crystallization conditions, substrate affinity is sufficiently tight to permit crystallographic analysis.

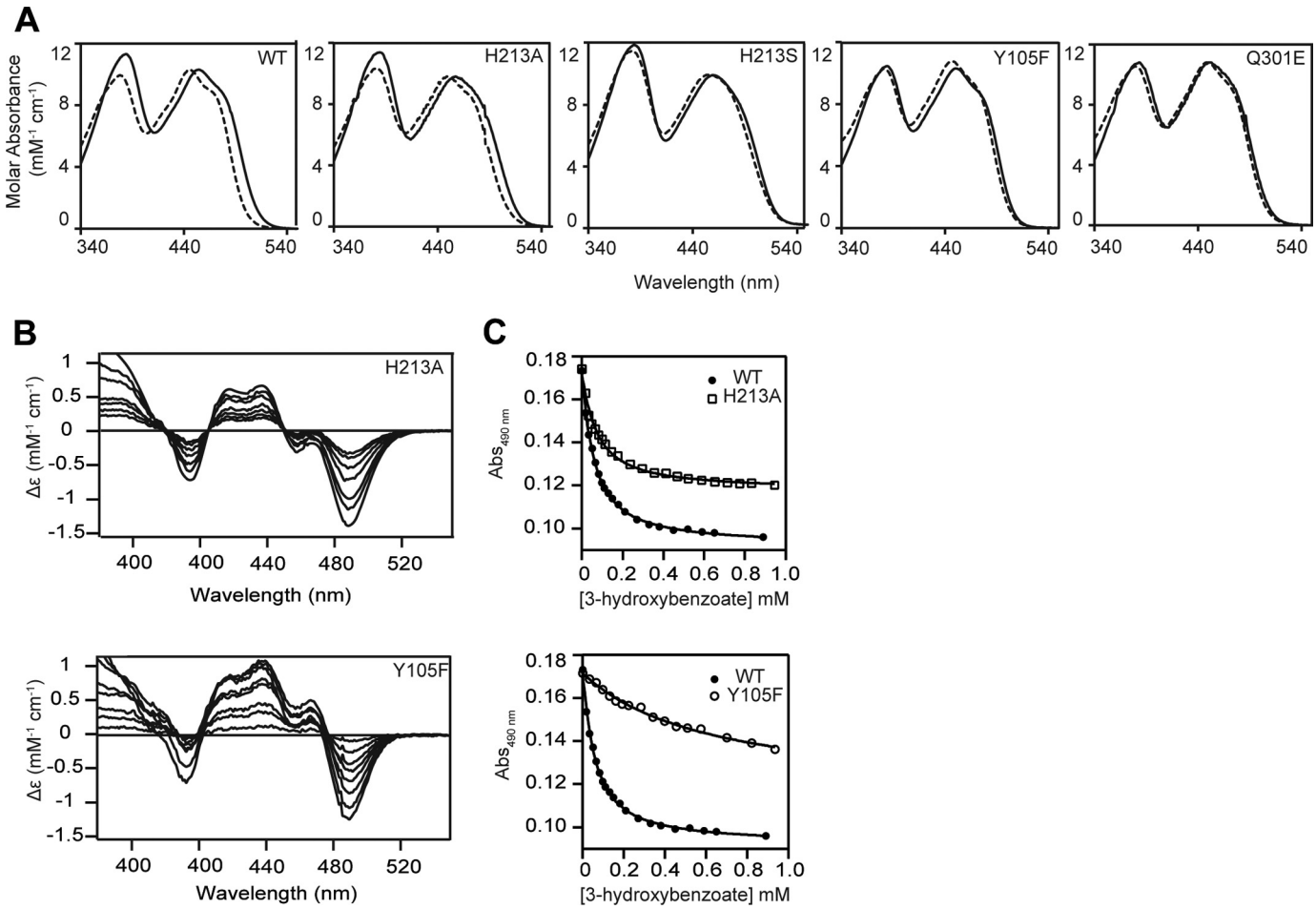

FIGURE 7. **Substrate binding properties of 3HB6H active site variants.** *A*, optical spectra of 3HB6H$_{WT}$, H213A, H213S, Y105F, and Q301E. *Solid line*, free enzyme; *dashed line*, enzyme in complex with 3-hydroxybenzoate (1.3 mM). *B*, absorbance (*Abs*) difference spectra of H213A and Y105F titrated with increasing substrate concentrations. For clarity, only selected spectra are shown. *C*, dissociation constants of H213A and Y105F variants compared with 3HB6H$_{WT}$. All spectra were recorded in 50 mM Tris-SO$_4$ (pH 8).

The Y105F and Q301E mutant structures are virtually identical to the native protein except for the side chain substitution. The network shown in Fig. 6*D* shows Tyr-105 hydrogen bonding to the carbonyl of Gln-49 whose amide hydrogen bonds to the carboxylate of the substrate. Eliminating the Tyr-Gln hydrogen bond could either make the amide less polarized, decreasing the partial positive charge on the nitrogen and causing a weaker hydrogen bond, or allow the amide to rotate 180° so that the carbonyl of the Gln faces the carboxylate, preventing the hydrogen bond. Collectively, these findings provide the foundation for defining a structural framework to substrate binding and hydroxylation.

DISCUSSION

Chloride Binding—A chloride ion was found to bind in front of the flavin ring in direct contact with the pyrimidine moiety of the cofactor and the NH backbone atoms of residues 304 and 305 (Fig. 4*A*). This binding site corresponds to the niche predicted to host the oxygen atoms of the flavin-hydroperoxide adduct formed upon reaction of the reduced flavin with oxygen. In this context, it is noticeable that many flavoprotein hydroxylases are inhibited by chloride ions (41, 42). For instance, studies with PHBH showed a competitive mode of inhibition with respect to NADPH and a mixed-type inhibition with respect to the physiological substrate 4-hydroxybenzoate (43). 3HB6H is no exception because it also exhibits similar mixed-type inhibition with chloride ions (Fig. 8). Collectively, these findings indicate that the negatively charged chlorine can both interfere with the binding and/or reactivity of the enzyme with oxygen, NADH, or both.

Lipid Binding—A non-covalently bound phospholipid molecule was found in each monomer of 3HB6H in the crystallographic model. The fatty acid chains occupy hydrophobic channels that deeply penetrate into the interior of the substrate-binding domain, whereas the hydrophilic portion of the molecule protrudes out of the protein surface, connecting the dimerization domains via a few interactions. Any attempt to natively remove the lipid from the protein by using beads (44), detergents, or reversible unfolding failed, indicating that the binding of the phospholipid is very strong. Interestingly, the flavoenzyme 6-hydroxy-L-nicotine oxidase from *Arthrobacter nicotinovorans* (45) also contains a similarly bound phospholipid molecule, which remains to be functionally characterized. In the case of 3HB6H, it is interesting to observe that the enzyme presents a different dimerization interface with respect to that of PHBH despite similar secondary structure organiza-

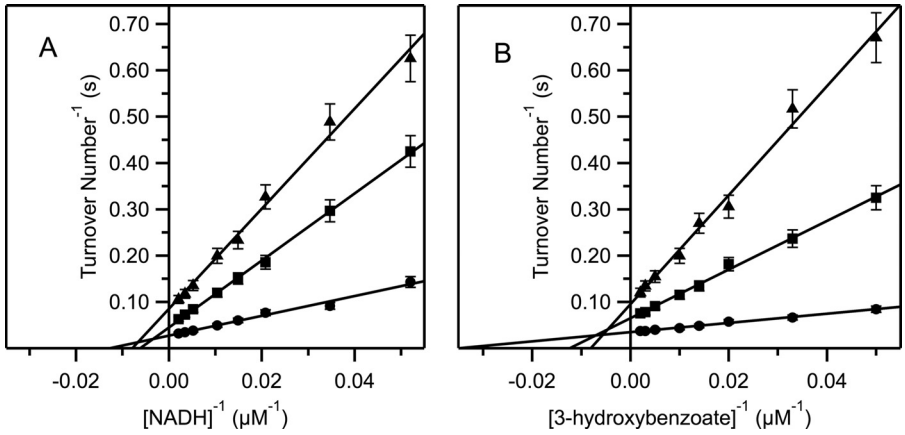

FIGURE 8. **Inhibition of 3HB6H by chloride ions.** *A*, Lineweaver-Burk plot of 3HB6H activity dependence on NADH concentration in the presence of 250 μM 3-hydroxybenzoate and 0 (*circles*), 20 (*squares*), and 40 mM NaCl (*triangles*), respectively. *B*, Lineweaver-Burk plot of 3HB6H activity dependence on 3-hydroxybenzoate concentration in the presence of 250 μM NADH and 0 (*circles*), 20 (*squares*), and 40 mM NaCl (*triangles*), respectively. *Error bars* represent S.E.

tion. Most of the hydrophobic residues involved in PHBH dimerization are not conserved in 3HB6H, and the few protein-protein interactions are primarily made by helix H13 contacts. We hypothesize that phospholipids in 3HB6H function as glue, promoting and stabilizing dimer formation. Recently, Clarke (46) and Ozeir *et al.* (47) have characterized a flavoprotein hydroxylase in *Saccharomyces cerevisiae* (Coq6) that is involved in coenzyme Q biosynthesis and is homologous to the *E. coli* UbiF, UbiH, and UbiI enzymes (48–50). Coq6, UbiF, and UbiI catalyze the *ortho*-hydroxylation of 4-hydroxybenzoic analogs containing a polyprenyl chain. UbiH catalyzes the *para*-hydroxylation of a similar lipophilic aromatic substrate. Flavoprotein hydroxylases acting on phenolic acids and aromatic redox-active lipids such as coenzyme Q could clearly derive from a common ancestor based on their evident structural homology and mechanistic similarity. A hypothesis is that the ability to bind aliphatic chains such as phospholipids and prenyl chains has been maintained (with different affinity) by 3HB6H, UbiF/H/I, and Coq6 and was lost by most other FAD-dependent hydroxylases. Alternatively, the capacity to bind aliphatic ligands arose independently during evolution of flavoprotein hydroxylases.

Substrate Binding—Elucidation of the interaction between 3HB6H and its physiological substrate is particularly interesting in relation to the regioselectivity of the hydroxylation reaction. One of two observed substrate orientations observed in the H213S structure most likely corresponds to the catalytically competent binding mode with the substrate C6 carbon (the site of hydroxylation) close to the flavin C4a (Fig. 6*D*). The carboxylate group of 3-hydroxybenzoate interacts with Gln-49 and Tyr-105, whereas its 3-hydroxyl group is engaged in H-bonds with His-213 and Gln-301 side chains. These features are fully consistent with the mutagenesis data. The properties of the Y105F variant indicate that disruption of the H-bond network involving Gln-49 can mildly perturb binding affinity without, however, affecting activation of the substrate (Table 4). Conversely, substitutions of Gln-301 with Glu and of His-213 with Ala or Ser render the enzyme inactive. These two side chains have a primary role in catalysis, possibly facilitating deprotonation of the substrate phenol. Indeed, a comparable mechanism of substrate activation occurs in PHBH where a hydrogen bond network that extends to the protein surface is involved in ionization of the substrate hydroxyl moiety (31).

Analysis of substrate binding highlights a most remarkable feature. The aromatic ring is in van der Waals contact with the terminal part of the fatty chain of the bound phospholipid, which is, therefore, an integral element of the substrate-binding site. Thus, 3-hydroxybenzoate binds through a three-point anchoring mechanism that relies on the His-213/Gln-301 pair for providing the substrate-activating H-bond partner to the 3-hydroxyl, on the Gln-49/Tyr-105 pair for interacting with the carboxylate group, and on the lipid tail for creating a solvent-excluded environment that embeds the more hydrophobic aromatic group of the ligand. Consistently, an additional OH group on the lipid-facing edge of the substrate ring makes the binding weaker (3,5-dihydroxybenzoate) or very poor (3,4-dihydroxybenzoate). Only the 2-hydroxyl group, which will bind opposite the lipid wall, can be fully tolerated with 2,3-dihydroxybenzoate, which is essentially as good a substrate as 3-hydroxybenzoate (14). This mode of affording selectivity is nicely illustrated by the comparison of 3HB6H with the substrate-bound structure of 3HB4H (Protein Data Bank code 2DKH). These two enzymes act on the same substrate but with different regioselectivities (6- *versus* 4-hydroxylation). The structural superposition (Fig. 6*D*) shows that the bound 3-hydroxybenzoate molecules are rotated with respect to each other around an axis orthogonal to the aromatic ring. The substrates are coplanar, but their differing orientations make C6 of the 3HB6H-bound ligand perfectly overlap with C4 of the 3HB4H-bound substrate. In this way, the respective sites of hydroxylation are at the proper distance and orientation from the oxygen-activating C4a atom of the flavin. This is a beautiful example of how enzymes can vary the regioselectivity of their reaction with the peculiarity that a tightly bound phospholipid is utilized to attain this effect.

Acknowledgment—We are grateful to Stefano Rovida for assistance during crystallization screening experiments.

REFERENCES

1. Montersino, S., Tischler, D., Gassner, G. T., and van Berkel, W. J. (2011) Catalytic and structural features of flavoprotein hydroxylases and epoxidases. *Adv. Synth. Catal.* **353,** 2301–2319
2. van Berkel, W. J., Kamerbeek, N. M., and Fraaije, M. W. (2006) Flavoprotein monooxygenases, a diverse class of oxidative biocatalysts. *J. Biotechnol.* **124,** 670–689
3. Palfey, B. A., and McDonald, C. A. (2010) Control of catalysis in flavin-dependent monooxygenases. *Arch. Biochem. Biophys.* **493,** 26–36
4. Schreuder, H. A., Prick, P. A., Wierenga, R. K., Vriend, G., Wilson, K. S., Hol, W. G., and Drenth, J. (1989) Crystal structure of the p-hydroxybenzoate hydroxylase-substrate complex refined at 1.9 Å resolution. Analysis of the enzyme-substrate and enzyme-product complexes. *J. Mol. Biol.* **208,** 679–696
5. Enroth, C., Neujahr, H., Schneider, G., and Lindqvist, Y. (1998) The crystal structure of phenol hydroxylase in complex with FAD and phenol provides evidence for a concerted conformational change in the enzyme and its cofactor during catalysis. *Structure* **6,** 605–617
6. Hiromoto, T., Fujiwara, S., Hosokawa, K., and Yamaguchi, H. (2006) Crystal structure of 3-hydroxybenzoate hydroxylase from *Comamonas testosteroni* has a large tunnel for substrate and oxygen access to the active site. *J. Mol. Biol.* **364,** 878–896
7. McCulloch, K. M., Mukherjee, T., Begley, T. P., and Ealick, S. E. (2009) Structure of the PLP degradative enzyme 2-methyl-3-hydroxypyridine-5-carboxylic acid oxygenase from *Mesorhizobium loti* MAFF303099 and its mechanistic implications. *Biochemistry* **48,** 4139–4149
8. Treiber, N., and Schulz, G. E. (2008) Structure of 2,6-dihydroxypyridine 3-hydroxylase from a nicotine-degrading pathway. *J. Mol. Biol.* **379,** 94–104
9. Greenhagen, B. T., Shi, K., Robinson, H., Gamage, S., Bera, A. K., Ladner, J. E., and Parsons, J. F. (2008) Crystal structure of the pyocyanin biosynthetic protein PhzS. *Biochemistry* **47,** 5281–5289
10. Koskiniemi, H., Metsä-Ketelä, M., Dobritzsch, D., Kallio, P., Korhonen, H., Mäntsälä, P., Schneider, G., and Niemi, J. (2007) Crystal structures of two aromatic hydroxylases involved in the early tailoring steps of angucycline biosynthesis. *J. Mol. Biol.* **372,** 633–648
11. Lindqvist, Y., Koskiniemi, H., Jansson, A., Sandalova, T., Schnell, R., Liu, Z., Mäntsälä, P., Niemi, J., and Schneider, G. (2009) Structural basis for substrate recognition and specificity in aklavinone-11-hydroxylase from rhodomycin biosynthesis. *J. Mol. Biol.* **393,** 966–977
12. Ryan, K. S., Howard-Jones, A. R., Hamill, M. J., Elliott, S. J., Walsh, C. T., and Drennan, C. L. (2007) Crystallographic trapping in the rebeccamycin biosynthetic enzyme RebC. *Proc. Natl. Acad. Sci. U.S.A.* **104,** 15311–15316
13. Volkers, G., Palm, G. J., Weiss, M. S., Wright, G. D., and Hinrichs, W. (2011) Structural basis for a new tetracycline resistance mechanism relying on the TetX monooxygenase. *FEBS Lett.* **585,** 1061–1066
14. Montersino, S., and van Berkel, W. J. (2012) Functional annotation and characterization of 3-hydroxybenzoate 6-hydroxylase from *Rhodococcus jostii* RHA1. *Biochim. Biophys. Acta* **1824,** 433–442
15. Chun, J., Kang, S. O., Hah, Y. C., and Goodfellow, M. (1996) Phylogeny of mycolic acid-containing actinomycetes. *J. Ind. Microbiol. Biotechnol.* **17,** 205–213
16. Finnerty, W. R. (1992) The biology and genetics of the genus *Rhodococcus*. *Annu. Rev. Microbiol.* **46,** 193–218
17. Gürtler, V., Mayall, B. C., and Seviour, R. (2004) Can whole genome analysis refine the taxonomy of the genus *Rhodococcus*? *FEMS Microbiol. Rev.* **28,** 377–403
18. van der Geize, R., and Dijkhuizen, L. (2004) Harnessing the catabolic diversity of rhodococci for environmental and biotechnological applications. *Curr. Opin. Microbiol.* **7,** 255–261
19. McLeod, M. P., Warren, R. L., Hsiao, W. W., Araki, N., Myhre, M., Fernandes, C., Miyazawa, D., Wong, W., Lillquist, A. L., Wang, D., Dosanjh, M., Hara, H., Petrescu, A., Morin, R. D., Yang, G., Stott, J. M., Schein, J. E., Shin, H., Smailus, D., Siddiqui, A. S., Marra, M. A., Jones, S. J., Holt, R., Brinkman, F. S., Miyauchi, K., Fukuda, M., Davies, J. E., Mohn, W. W., and Eltis, L. D. (2006) The complete genome of *Rhodococcus* sp. RHA1 provides insights into a catabolic powerhouse. *Proc. Natl. Acad. Sci. U.S.A.* **103,** 15582–15587
20. Evans, P. (2006) Scaling and assessment of data quality. *Acta Crystallogr. D Biol. Crystallogr.* **62,** 72–82
21. Collaborative Computational Project, Number 4 (1994) The CCP4 suite: programs for protein crystallography. *Acta Crystallogr. D Biol. Crystallogr.* **50,** 760–763
22. Sheldrick, G. M. (2010) Experimental phasing with SHELXC/D/E: combining chain tracing with density modification. *Acta Crystallogr. D Biol. Crystallogr.* **66,** 479–485
23. Langer, G., Cohen, S. X., Lamzin, V. S., and Perrakis, A. (2008) Automated macromolecular model building for x-ray crystallography using ARP/wARP version 7. *Nat. Protoc.* **3,** 1171–1179
24. Murshudov, G. N., Skubák, P., Lebedev, A. A., Pannu, N. S., Steiner, R. A., Nicholls, R. A., Winn, M. D., Long, F., and Vagin, A. A. (2011) REFMAC5 for the refinement of macromolecular crystal structures. *Acta Crystallogr. D Biol. Crystallogr.* **67,** 355–367
25. Emsley, P., Lohkamp, B., Scott, W. G., and Cowtan, K. (2010) Features and development of Coot. *Acta Crystallogr. D Biol. Crystallogr.* **66,** 486–501
26. DeLano, W. L. (2010) *The PyMOL Molecular Graphics System*, Version 1.3r1, Schrödinger, LLC, New York
27. McNicholas, S., Potterton, E., Wilson, K. S., and Noble, M. E. (2011) Presenting your structures: the CCP4mg molecular-graphics software. *Acta Crystallogr. D Biol. Crystallogr.* **67,** 386–394
28. Karplus, P. A., and Diederichs, K. (2012) Linking crystallographic model and data quality. *Science* **336,** 1030–1033
29. Eppink, M. H., Schreuder, H. A., and van Berkel, W. J. (1997) Identification of a novel conserved sequence motif in flavoprotein hydroxylases with a putative dual function in FAD/NAD(P)H binding. *Protein Sci.* **6,** 2454–2458
30. Entsch, B., Cole, L. J., and Ballou, D. P. (2005) Protein dynamics and electrostatics in the function of p-hydroxybenzoate hydroxylase. *Arch. Biochem. Biophys.* **433,** 297–311
31. Entsch, B., and van Berkel, W. J. (1995) Structure and mechanism of para-hydroxybenzoate hydroxylase. *FASEB J.* **9,** 476–483
32. Eppink, M. H., Schreuder, H. A., and van Berkel, W. J. (1998) Interdomain binding of NADPH in *p*-hydroxybenzoate hydroxylase as suggested by kinetic, crystallographic and modeling studies of histidine 162 and arginine 269 variants. *J. Biol. Chem.* **273,** 21031–21039
33. Wang, J., Ortiz-Maldonado, M., Entsch, B., Massey, V., Ballou, D., and Gatti, D. L. (2002) Protein and ligand dynamics in 4-hydroxybenzoate hydroxylase. *Proc. Natl. Acad. Sci. U.S.A.* **99,** 608–613
34. Eppink, M. H., Overkamp, K. M., Schreuder, H. A., and Van Berkel, W. J. (1999) Switch of coenzyme specificity of p-hydroxybenzoate hydroxylase. *J. Mol. Biol.* **292,** 87–96
35. Montersino, S., Golovleva, L., Schlömann, M., and van Berkel, W. J. H. (2008) in *Flavins and Flavoproteins* (Frago, S., Gomez-Moreno, C., and Medina, M., eds) pp. 51–56, Prensas Universitarias de Zaragoza, Zaragoza, Spain
36. Weijer, W. J., Hofsteenge, J., Beintema, J. J., Wierenga, R. K., and Drenth, J. (1983) p-Hydroxybenzoate hydroxylase from *Pseudomonas fluorescens*. 2. Fitting of the amino-acid sequence to the tertiary structure. *Eur. J. Biochem.* **133,** 109–118
37. Fahy, E., Cotter, D., Sud, M., and Subramaniam, S. (2011) Lipid classification, structures and tools. *Biochim. Biophys. Acta* **1811,** 637–647
38. Fahy, E., Subramaniam, S., Murphy, R. C., Nishijima, M., Raetz, C. R., Shimizu, T., Spener, F., van Meer, G., Wakelam, M. J., and Dennis, E. A. (2009) Update of the LIPID MAPS comprehensive classification system for lipids. *J. Lipid Res.* **50,** S9–S14
39. Oursel, D., Loutelier-Bourhis, C., Orange, N., Chevalier, S., Norris, V., and Lange, C. M. (2007) Lipid composition of membranes of *Escherichia coli* by liquid chromatography/tandem mass spectrometry using negative electrospray ionization. *Rapid Commun. Mass Spectrom.* **21,** 1721–1728
40. Pulfer, M., and Murphy, R. C. (2003) Electrospray mass spectrometry of phospholipids. *Mass Spectrom. Rev.* **22,** 332–364
41. van Berkel, W. J., and Müller, F. (1991) in *Chemistry and Biochemistry of Flavoenzymes* (Müller, F., ed) Vol. 2, pp. 2–29, CRC Press, Boca Raton, FL
42. Van Berkel, W. J., and Van Den Tweel, W. J. (1991) Purification and char-

acterisation of 3-hydroxyphenylacetate 6-hydroxylase: a novel FAD-dependent monooxygenase from a *Flavobacterium* species. *Eur. J. Biochem.* **201,** 585–592
43. Steennis, P. J., Cordes, M. M., Hilkens, J. H., and Müller, F. (1973) On the interaction of para-hydroxybenzoate hydroxylase from *Pseudomonas fluorescens* with halogen ions. *FEBS Lett.* **36,** 177–180
44. Crawford, J. M., Korman, T. P., Labonte, J. W., Vagstad, A. L., Hill, E. A., Kamari-Bidkorpeh, O., Tsai, S.-C., and Townsend, C. A. (2009) Structural basis for biosynthetic programming of fungal aromatic polyketide cyclization. *Nature* **461,** 1139–1143
45. Kachalova, G. S., Bourenkov, G. P., Mengesdorf, T., Schenk, S., Maun, H. R., Burghammer, M., Riekel, C., Decker, K., and Bartunik, H. D. (2010) Crystal structure analysis of free and substrate-bound 6-hydroxy-L-nicotine oxidase from *Arthrobacter nicotinovorans*. *J. Mol. Biol.* **396,** 785–799
46. Clarke, C. F. (2011) Coq6 hydroxylase: unmasked and bypassed. *Chem. Biol.* **18,** 1069–1070
47. Ozeir, M., Mühlenhoff, U., Webert, H., Lill, R., Fontecave, M., and Pierrel, F. (2011) Coenzyme Q biosynthesis: Coq6 is required for the C5-hydroxylation reaction and substrate analogs rescue Coq6 deficiency. *Chem. Biol.* **18,** 1134–1142
48. Kwon, O., Kotsakis, A., and Meganathan, R. (2000) Ubiquinone (coenzyme Q) biosynthesis in *Escherichia coli*: identification of the ubiF gene. *FEMS Microbiol. Lett.* **186,** 157–161
49. Meganathan, R. (2001) Ubiquinone biosynthesis in microorganisms. *FEMS Microbiol. Lett.* **203,** 131–139
50. Hajj Chehade, M., Loiseau, L., Lombard, M., Pecqueur, L., Ismail, A., Smadja, M., Golinelli-Pimpaneau, B., Mellot-Draznieks, C., Hamelin, O., Aussel, L., Kieffer-Jaquinod, S., Labessan, N., Barras, F., Fontecave, M., and Pierrel, F. (2013) *ubiI*, a new gene in *Escherichia coli* coenzyme Q biosynthesis, is involved in aerobic C5-hydroxylation. *J. Biol. Chem.* **288,** 20085–20092
51. Holm, L., and Rosenström, P. (2010) Dali server: conservation mapping in 3D. *Nucleic Acids Res.* **38,** W545–W549
52. Gille, C., and Frömmel, C. (2001) STRAP: editor for STRuctural Alignments of Proteins. *Bioinformatics* **17,** 377–378
53. Thompson, J. D., Higgins, D. G., and Gibson, T. J. (1994) CLUSTAL W: improving the sensitivity of progressive multiple sequence alignment through sequence weighting, position-specific gap penalties and weight matrix choice. *Nucleic Acids Res.* **22,** 4673–4680